Available online at www.sciencedirect.com
SCIENCE DIRECT®
Journal of the European Ceramic Society 25 (2005) 301–311
www.elsevier.com/locate/jeurceramsoc

Mechanical and microstructural characterization of calcium aluminosilicate (CAS) and SiO_2/CAS composites deformed at high temperature and high pressure

Shaocheng Ji [a,d,*], Erik Rybacki [b], Richard Wirth [b], Zhenting Jiang [c], Bin Xia [d]

[a] *Département des Génies Civil, Géologique et des Mines, École Polytechnique de Montréal, Montréal, Canada H3C 3A7*
[b] *GeoForschungsZentrum Potsdam, D-14473 Potsdam, Germany*
[c] *Department of Earth Sciences, University of Liverpool, Liverpool L69 3BX, UK*
[d] *Laboratory of Marginal Sea Geology, Guangzhou Institute of Geochemistry and South China Sea Institute of Oceanography, Chinese Academy of Sciences, Wushan, Guangzhou 510640, PR China*

Received 16 October 2003; received in revised form 18 February 2004; accepted 25 February 2004
Available online 21 July 2004

Abstract

We performed axial compression experiments on polycrystalline calcium aluminosilicate (CAS or anorthite) and on particulate and layered composites with equal volume fractions of CAS and SiO_2 (quartz) at a confining pressure of 300 MPa, temperatures of 1173–1473 K, and strain rates of 10^{-5} to $10^{-4}\,s^{-1}$. The dense samples were fabricated from quartz crystalline and CAS glass powders by hot isostatic pressing (HIP). Under the experimental conditions, triclinic CAS, regardless in monolithic aggregates or composites, deforms by dislocation creep as indicated by TEM microstructures, intensive grain boundary migration recrystallization and strong crystallographic preferred orientation (CPO). Dislocation creep of CAS is characterized by dominant glide on a single slip system (0 1 0)[1 0 0] while mechanical twinning, anisotropic growth and recrystallization play an role to relieve the strain incompatibilities which would otherwise result from such limited slip systems. Particulate and particularly layered composites are significantly stronger than monolithic CAS aggregates, indicating that quartz is an effective reinforcement to the CAS matrix even when the material is used at high temperature and high pressure. Under layer-normal compression, the flow strength of layered composites increases remarkably with decreasing the thickness of the layers, and the thin-layered composites are significantly stronger than particulate counterparts with the same composition. The observed layering-induced stiffening is due to constraint effects of rigid quartz on plastic flow of CAS.

Keywords: Composites; Mechanical properties; Hot isostatic pressing; Plasticity; Anorthite; SiO_2

1. Introduction

In this paper we present our experimental results on the mechanical properties and microstructures of monolithic calcium aluminosilicate (CAS or anorthite: $CaAl_2Si_3O_8$) aggregates, particulate and layered composites with equal volume fractions of quartz (SiO_2) and CAS, deformed in axial compression ($\sigma_1 > \sigma_2 = \sigma_3 > 0$, where σ_1, σ_2, σ_3 are the maximum, intermediate and least compressive principal stresses, respectively) at temperatures of 1173–1473 K, strain rates of 10^{-5} to $10^{-4}\,s^{-1}$ and a constant confining pressure of 300 MPa. Two main considerations on the merit of this study should be mentioned in the following:

(1) The CAS has been widely used as a matrix in fibre- or particle-reinforced ceramic composites that are excellent prospective materials for application as mechanical components in aerospace and automobile propulsion and power systems.[1–4] For better fabrication and application of such composites, it is essential to understand the rheological properties, microstructures and textures of the CAS and various CAS-based ceramic composites deformed under various conditions (*T*, *P*, flow strength and strain rate). Although a significant amount of work has

* Corresponding author. Tel.: +1-514-3404711x5134; fax: +1-514-3403970.
E-mail address: sji@polymtl.ca (S. Ji).

0955-2219/$ – see front matter © 2004 Elsevier Ltd. All rights reserved.
doi:10.1016/j.jeurceramsoc.2004.02.018

been carried out on monolithic CAS and other plagioclase feldspars under uniaxial compression ($\sigma_1 > \sigma_2 = \sigma_3 = 0$) at ambient pressure,[5–11] it remains uncertain if the results from small strain creep tests are able to be extrapolated to other conditions because a small amount of strain is usually insufficient for steady-state microstructure to occur.[12] Cavitation often occurs in the samples deformed at ambient pressure.[5–11] Furthermore, the application of CAS-based ceramic composites to a high temperature and high pressure environment was largely hindered by the relatively little knowledge of mechanical, microstructural and textural data of CAS and CAS-based composites from laboratory tests.[11,13–16]

(2) CAS crystal is triclinic with the lowest crystallographic symmetry. The relative activity of different slip systems and dynamic recrystallization in dislocation creeping CAS under varying physical and chemical conditions are still poorly known. The investigation of CAS microstructure and texture can further our understanding of plastic deformation mechanism and textural development in triclinic crystalline materials. In spite of its importance, CAS has a much smaller textural database than other crystalline materials such as metals and minerals (mainly olivine, quartz and calcite). Reasons for this are purely technical because CAS is triclinic. Full crystallographic orientations of CAS cannot be determined using conventional X-ray due to the large number of overlapping diffraction peaks. The texture of triclinic albite ($NaAlSi_3O_8$) has been measured by employing synchrotron X-ray goniometry,[17] but this technique is expensive and not widely available. Neutron diffraction goniometry has been applied to the measurements of plagioclase texture,[18,19] however, relatively large volumes of sample material (>1 cm^3 which is often larger than most of samples deformed experimentally[8–11]) are needed for this type of measurements because neutron flux densities are generally low. CAS texture can be determined using optical U-stage method[18,20], but its grain size should be larger than 20–30 μm and the measurement is time-consuming. Recently, it was shown that the most powerful technique for successfully measuring texture of triclinic crystals is electron backscattering diffraction (EBSD) equipped in a scanning electron microscope (SEM).[21–23] Thus, this new technique was used in collecting representative CAS texture from our deformed samples.

2. Samples

Four categories of samples were prepared, using hot isostatic pressing (HIP) techniques, for mechanical tests. They are layered composites (LC, Fig. 1), particulate composites (PC, Fig. 2a) of quartz (Qtz) and CAS, and the pure CAS (Fig. 2b) and Qtz (Fig. 2c) polycrystalline aggregates. The LC contains alternating Qtz and CAS layers with strong

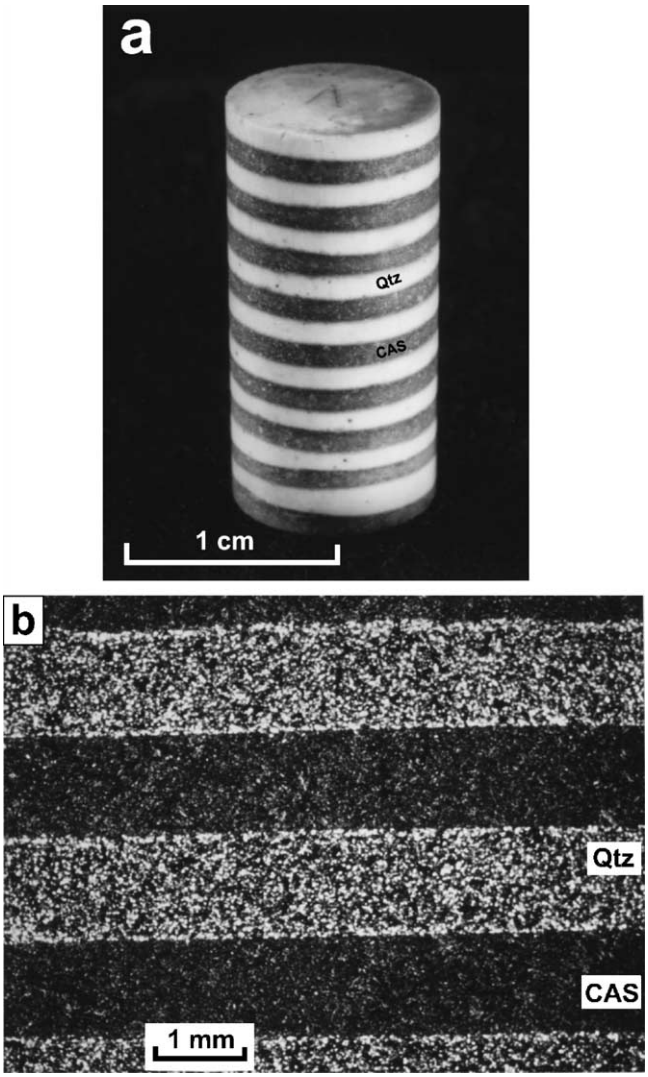

Fig. 1. Photograph (a) and photomicrograph (b) of a hot isostatical pressed layered Qtz–CAS composite.

and sharp interfaces (Fig. 1), which was created during cold pressing and subsequently thinned during HIP. The layering in cylindrical LC samples is characterized by the ratio of the diameter (d) to the thickness (h) of material layers. The PC is a homogeneous mixture of equal volume fraction of Qtz and CAS (Fig. 2a).

Commercial powders of CAS ($An_{98.9}Or_{0.2}Ab_{0.9}$) glass (Schott GmbH, Germany) and quartz (Johnson-Matthey GmbH, Germany) were used as the starting materials. The same CAS glass powder has been used in previous studies.[16,22] The CAS glass powder with particle size less than <60 μm was first predried in an oven at a constant temperature of 393 K for at least 100 h to drive off adsorbed water. The powder was then encapsulated into a steel jacket ($\phi = 15$ mm, $l = 25$ mm) and cold-pressed under an axial stress of about 150 MPa. Each cold-pressed pellet was HIPed and statistically annealed at 1123 K for 1 h, 1323 K for 1 h and then 1473 K for 3 h at a confin-

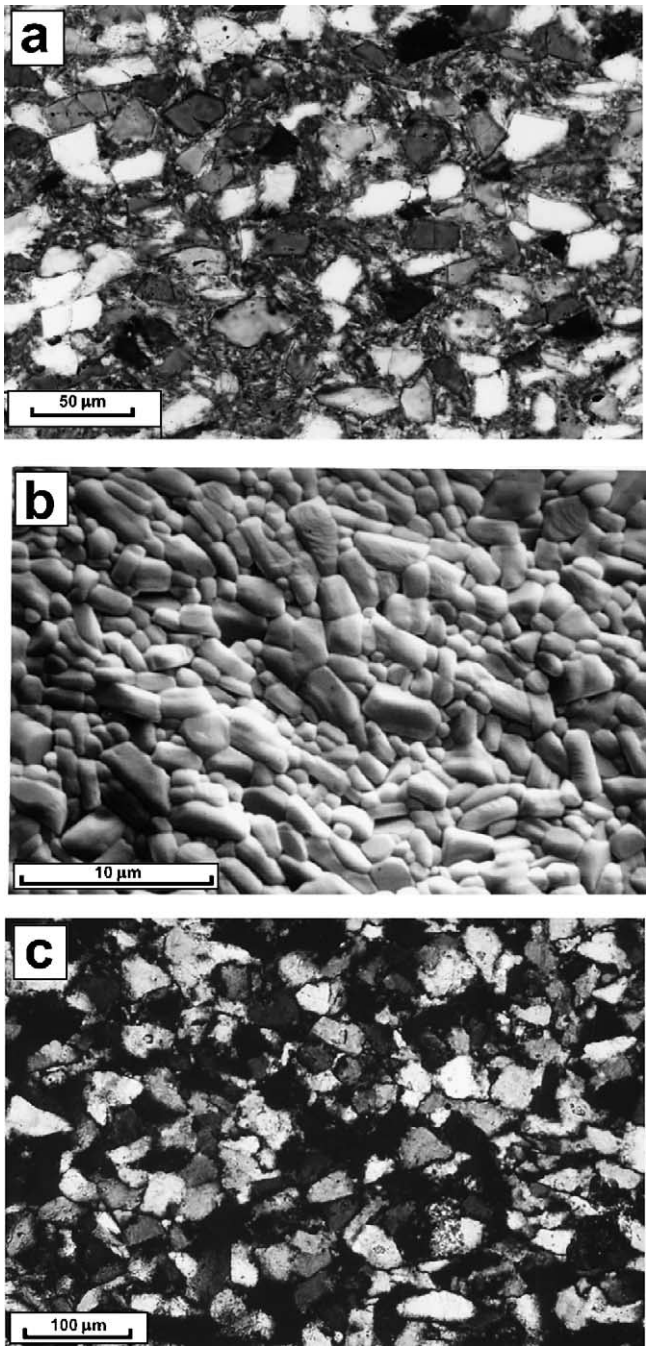

Fig. 2. Hot isostatical pressed but undeformed Qtz–CAS particulate composite (a), pure CAS aggregate (b) and pure quartz (Qtz) aggregate (c). (a and c) Optical micrograph of petrographic thin sections. (b) SEM micrograph of a spherulite-free area from a polished and thermally etched (1373 K, 30 h) sample.

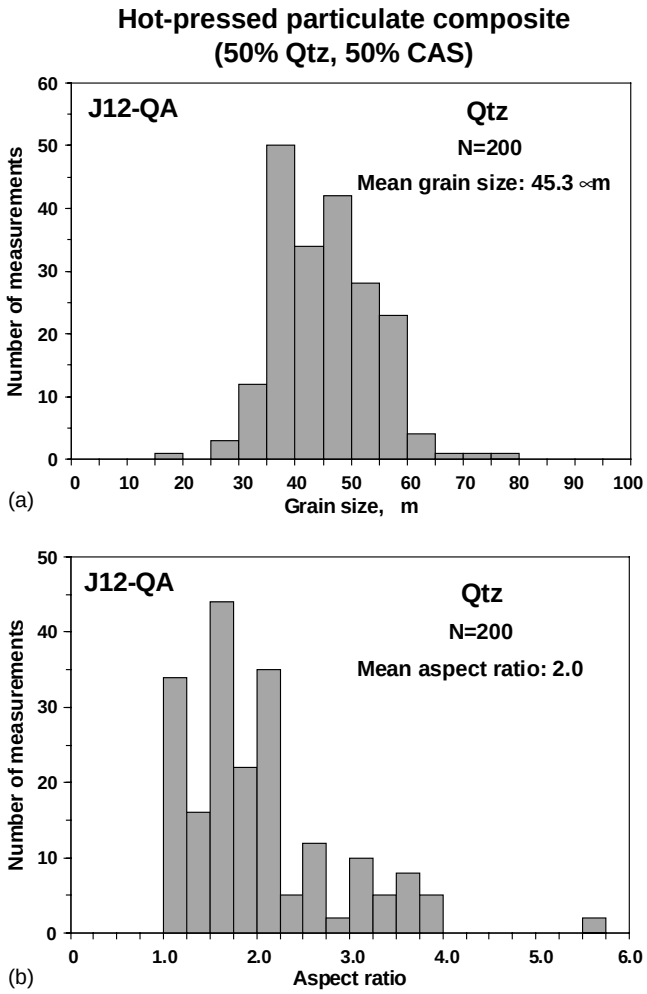

Fig. 3. Grain size distribution of quartz in a hot pressed particulate composite (J12-QA) consisting of 50 vol.% Qtz and 50 vol.% CAS. Measurements were made from optical photomicrographs.

ing pressure of 300 MPa to maximize the densification and to allow the polycrystalline aggregate starting toward microstructural equilibrium. After samples were retrieved from the vessel, the steel jacket was dissolved in a mixture of 50/50 vol.% HCl/HNO_3 acids. Density of each specimen was determined using Archimedes' method with the accuracy of $\pm 0.003\,g/cm^3$. Porosity is <1% in the HIPed CAS aggregates and Qtz–CAS particulate composites, 3–5% in the layered composites and 5–6% in the monolithic Qtz aggregates.

From two typical HIPed samples from each category, several polished thin sections were made for characterizing grain size, microstructure and water content of undeformed materials using optical microscope, SEM, transmission electron microscope (TEM), Fourier transform infrared spectrometer (FTIR) and EBSD analyses.

(1) Grain sizes of Qtz and CAS in the HIPed samples were measured using the linear intercept method[24] from petrographic sections and SEM (Zeiss DSM 962, GFZ-Potsdam, Germany) photographs of polished sections, respectively. Qtz displays a normal distribution of grain size ranging from 15 to 80 μm with a mean size of 45 μm (Fig. 3a). The distribution of Qtz grain aspect ratios is shown in Fig. 3b, yielding a mean value of 2.0. The CAS crystals, with a mean aspect ratio of 2.2 (Fig. 4b), display a log-normal distribution of grain

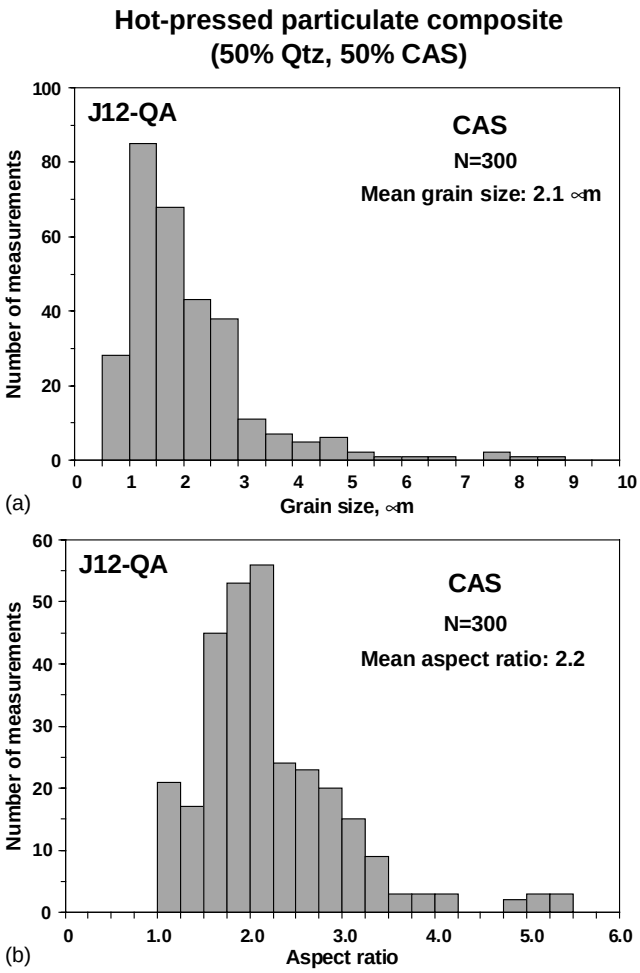

Fig. 4. Grain size distribution of CAS in hot pressed particulate composite (sample J12-QA) consisting of 50 vol.% Qtz and 50 vol.% CAS). Measurements were made from SEM photomicrographs.

size ranging from 0.4 to 9 μm with a mean value of 2.1 μm (Fig. 4a).

(2) Both optical and SEM observations show that Qtz grains in the PC aggregates form almost rigid clasts dispersed homogeneously within a relatively continuous matrix of CAS (Fig. 2a). Spherulites with radial fibres of CAS (not shown in Fig. 2) are occasionally observed in the pure CAS aggregates and the CAS layers of laminated composites. In the spherulites, CAS fibres are generally tabular on {0 1 0} with an elongation mainly along [0 0 1] and to a lesser extent along [1 0 0]. However, no CAS spherulites occur in particulate composites (Fig. 2a). It is generally accepted that spherulite texture results where the rate of crystal growth exceeds that of crystal nucleation[25–27]. The spherulite is a typical texture for crystallization of CAS glass that generally starts from a nucleation centre where the water content is relatively high. The volume fraction of spherulites in CAS aggregates is about 10% on average.

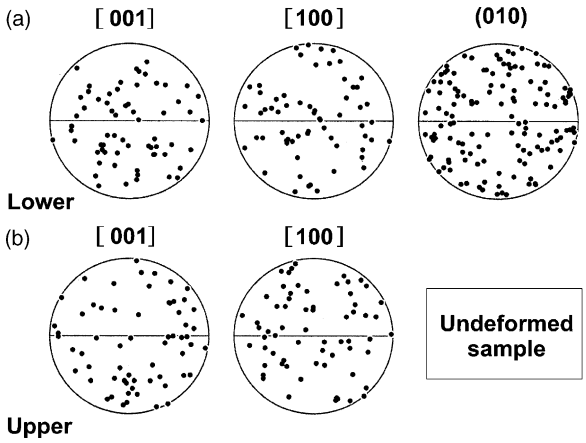

Fig. 5. Preferred orientations of triclinic CAS (0 1 0), [1 0 0] and [0 0 1] for undeformed, hot isostatical pressed, pure CAS aggregate (sample J7). Notice that the whole sphere, rather than a hemisphere, is necessary to represent the distribution of the positive directions. Projections on the lower (a) and upper (b) hemispheres. Stereonets are equal-area plots; 130 measurements are used.

(3) TEM (Philips CM200, GFZ-Potsdam, Germany) operating at 200 kV shows that the grain boundaries in the CAS aggregates are coherent and high-angle ones. They are straight and clean, suggesting that the crystallization and compaction of samples were well done.[16] Very little melt (<<0.5%) were found to occur in the triple-junctions. CAS grains in the HIPed samples are characterized by closely spaced growth twin lamellae with low dislocation densities ($\sim 10^{11}$ m^{-2}). The twins have their composition planes parallel to (0 1 0) and are mainly albite, Carlsbad and Carlsbad-albite types. The large fibres in CAS spherulites are actually composed of very small grains.[22]

(4) EBSD patterns of CAS and Qtz were measured and indexed using a SEM (Philips XL30) at Liverpool University, and the software package Channel + from HKL Software Company. The patterns were recorded at 30 kV acceleration voltage and nominal beam currents of 80 μA. No carbon coat was used on the thin sections, which were chemically–mechanically polished to remove specimen surface damage, because the coat deteriorated the EBSD image quality. In most cases, more than five or six bands were detected, allowing the bands indexed unambiguously by the computer simulation. The measurement uncertainty was given by the software as a mean angular deviation (MAD) between detected bands and simulated patterns. The indexing was not accepted if the MAD value was larger than 2°. EBSD measurements showed a random crystallographic preferred orientation (CPO) of either CAS (Fig. 5) or Qtz in HIPed samples, as expected for hydrostatic conditions.

(5) FTIR measurements using a Bruker IFS-66v (GFZ-Potsdam, Germany) show that the HIPed samples have a water content ranging from 8000 to 20,000 H/10^{6}Si with an average value of 13,000 H/10^{6}Si (~0.08 wt.%).

No significant difference in water content of samples before and after experimental deformation, indicating no detected loss of water species such as hydrogen through the Fe jacket during the mechanical tests.[16] If the water content were higher than 0.5 wt.%, solution-precipitation processes might operate as a creep mechanism in fine-grained feldspar.[15]

3. Mechanical data

All axial compressive tests ($\sigma_1 > \sigma_2 = \sigma_3 > 0$) were performed at 300 MPa confining pressure in a Paterson-type gas-medium apparatus (GFZ-Potsdam, Germany). Temperature varied from 1173 to 1473 K and axial strain rate from 10^{-5} to $10^{-4}\,s^{-1}$. Cylindrical specimens of 10 mm diameter and 20 mm length, fabricated from HIP, were jacketed in iron with 0.23 mm thick wall. The tests were carried out at constant strain rates. In this case, the sample flow strength corresponds to a differential stress of magnitude ($\sigma = \sigma_1 - \sigma_3$) which is superimposed upon a state of hydrostatic stress or confining pressure ($\sigma_2 = \sigma_3$). In other words, a differential stress (σ) is the difference between the maximum and minimum compressive principal stresses ($\sigma_1 - \sigma_3$). Thus it is always a positive scalar quantity. The axial compression is frequently used in laboratory experiments on the high temperature, high pressure properties of materials, minerals and rocks. Differential stresses and axial strains were derived, respectively, from measured loads and displacements after correcting for the load supported by the Fe jacket, rig distortion and change in sample cross-sectional area and length. The uncertainty in stress measurements is estimated within ±5 MPa. Temperature control was ±3 K along the gauge length of specimens.

Fig. 6 shows differential stress–strain curves for CAS aggregates from the sequence of axial compression tests at a constant rate of $10^{-5}\,s^{-1}$ and a confining pressure of 300 MPa at temperatures from 1273 to 1473 K. The shape of the stress–strain curves is characterized by an initial rapid strength increase followed by a slow strain hardening. At an axial strain of 0.25, the CAS polycrystal has flow strength of 16.6, 60.8 and 115.4 MPa at 1473, 1373 and 1273 K, respectively.

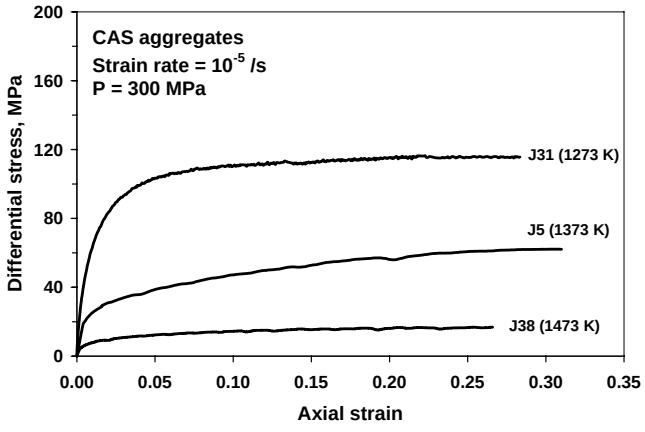

Fig. 6. Stress–strain curves for pure CAS aggregates deformed under axial compression at a confining pressure of 300 MPa, a constant strain rate of $10^{-5}\,s^{-1}$ and temperatures of 1273, 1373 and 1473 K.

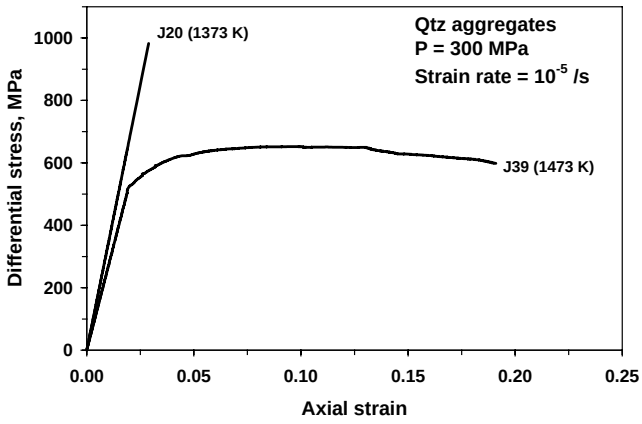

Fig. 7. Stress–strain curves for pure quartz aggregates deformed under axial compression at a confining pressure of 300 MPa, a constant strain rate of $10^{-5}\,s^{-1}$ and temperatures of 1373 and 1473 K. Note that the quartz aggregate could not yield at 1373 K or lower temperatures under the experimental conditions.

The polycrystalline aggregates of quartz, in spite of its porosity up to 5–6%, do not yield at 1273 and 1373 K at the conditions of confining pressure 300 MPa and strain rate $10^{-5}\,s^{-1}$ (Fig. 7). Even at a temperature as high as 1473 K, the quartz aggregate still has its strength higher than 600 MPa. Under the same conditions (1473 K, 300 MPa and $10^{-5}\,s^{-1}$), quartz is stronger than CAS by a factor of 40 ($\varepsilon = 0.15$) to 51 ($\varepsilon = 0.05$). There is thus a large rheological contrast between quartz ("hard" component) and CAS ("soft" component). It is expected that the addition of hard quartz into a soft matrix of CAS should produce significant effects on improving the mechanical properties of CAS–matrix ceramic composites.

Fig. 8 displays typical stress–strain curves for particulate composite that is a homogeneous mixture of equal volume fractions of Qtz and CAS. Three aspects of the mechanical data are striking: (i) Steady-state flow is only attained only in sample J9 which deformed at 1473 K and $10^{-5}\,s^{-1}$. (ii) A drastic drop in stress occurs immediately after a strength peak at a strain of approximately 0.04 for sample J26 that deformed at 1373 K and $10^{-4}\,s^{-1}$. The abrupt decrease in the level of stress supported from 389 MPa at $\varepsilon = 0.04$ to 160 MPa at $\varepsilon = 0.29$ is due to strong strain localization into a semi-brittle shear zone aligned at about 30° to the maximum compression stress (σ_1). (iii) Strain softening after a strength peak takes place in all samples deformed at 1173–1373 K and 1.0×10^{-5} to $2.5 \times 10^{-5}\,s^{-1}$. For example, the strength of sample J25, deformed at 1373 K and $2.5 \times 10^{-5}\,s^{-1}$, is 259, 214, 183 and 154 MPa at 0.10, 0.35, 0.50 and 0.65 strain, respectively. From 0.10 to 0.65 shortening strain, the

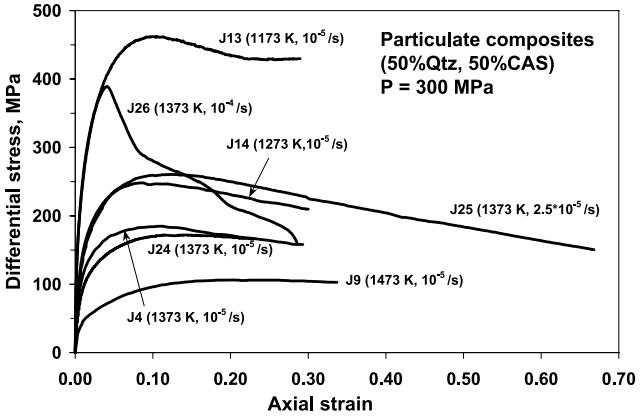

Fig. 8. Stress–strain curves for particulate composites containing equal volume fractions of quartz and CAS, deformed under axial compression at a confining pressure of 300 MPa, strain rates of 10^{-5}, 2.5×10^{-5} and $10^{-4}\,s^{-1}$, and temperatures of 1173, 1273, 1373 and 1473 K.

strength of the Qtz–CAS particle composite reduces about 40%. The coefficient of strain softening, $d\sigma/d\varepsilon$, at lower temperature or higher strain rate is larger than at higher temperature or lower strain rate. Comparison of Fig. 8 with Fig. 6 reveals that the PC samples are much stronger than the pure CAS aggregates. At a constant strain rate of $10^{-5}\,s^{-1}$, the maximum flow strength of PC samples is about two, three and six times higher than that of CAS aggregate at 1273, 1373 and 1473 K, respectively. Therefore, quartz is an effective reinforcement to the CAS matrix particularly when the composite material used at high temperatures.

Representative compressive stress–strain curves for LC samples deformed by layering-normal compression at a confining pressure of 300 MPa and a strain rate of $10^{-5}\,s^{-1}$ are shown in Fig. 9. Inspection of these curves reveals the following features: (i) Flow strength of the layered composites decreases with increasing temperature, as shown by the comparison among samples J1 (1473 K), J2 (1373 K) and J15 (1273 K). (ii) The bulk flow strength of the layered composites increases with increasing d/h ratio even though the volume fractions of Qtz and CAS are constant (Fig. 9). For example, the samples with $d/h = 9$ are significantly stronger than those with $d/h = 3$, and the latter are also stronger than the samples with $d/h = 1$. It is important to note that the layered composites with $d/h = 3$ have a flow strength similar to the particle composites deformed under the same conditions. Furthermore, all the layered composites are consistently stronger than the pure CAS aggregates although the CAS forms continuous layers normal to σ_1. The difference in the bulk flow strength between samples J22 and J40X is due to the following fact: J22 consists of a 10 mm thick layer of CAS between two 5 mm thick layers of Qtz while J40X is composed of a 10 mm thick layer of Qtz between two 5 mm thick layers of CAS. This indicates that the concentration of soft material such as CAS into a single thicker layer results in remarkable softening at higher strains.

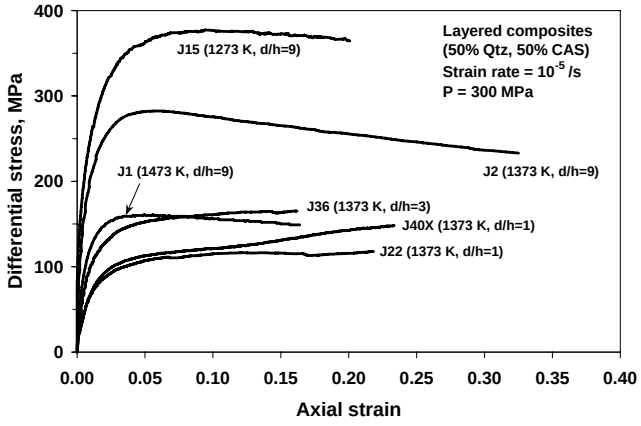

Fig. 9. Stress–strain curves for layered composites containing equal volume fractions of quartz and CAS, deformed under axial compression at a confining pressure of 300 MPa, a constant strain rate of $10^{-5}\,s^{-1}$, and temperatures of 1273, 1373 and 1473 K; *d* and *h* are the diameter and thickness of material layer, respectively.

4. Microstructures

The CAS aggregates and particularly the CAS layers in the deformed Qtz–CAS layered composites are intensively deformed with well-developed foliation (Fig. 10a), the latter is defined by preferential alignment of CAS lath-shaped crystals and polycrystalline ribbons or fibers. The spherulites, which initially had a spherical shape in HIPed CAS aggregates or layers within the layered composites (Fig. 10a), become oblate-ellipsoidal in the deformed specimens with their major axes in the foliation plane and minor axes parallel to the compressive direction (σ_1). The variation in spherulite shape displays a spatial variation of strain in each individual CAS layer of deformed LC samples: lower strain near the upper and lower boundaries of the layer and higher strain in the central part of the layer (Fig. 10a). At large shortening strains (>∼20%), the spherulites were recrystallized into very fine neograins and the recrystallization generally started first from the center of spherulites and from the spherulite boundaries at high angles to σ_1.

The texture of CAS from a CAS layer within a layered composite (sample J22) was measured using the EBSD technique.[21–23] This CAS layer achieved an average shortening strain of 52%. Grid measurements with 40 μm spacing were made across the central part of the CAS layer (Fig. 10a), where the accumulated strain is maximum. As shown in Fig. 11, the (0 1 0) poles display a strong concentration around the σ_1 direction while the [1 0 0] directions are preferentially aligned in the foliation plane perpendicular to σ_1. Both [0 0 1] directions and (0 0 1) poles are scattered. The CPO pattern can be interpreted as a result of dislocation slip on the (0 1 0)[1 0 0] system. If anisotropic growth of CAS under the axially compressive strain field were the mechanism for the CPO formation, the [0 0 1] direction should be aligned in the foliation plane perpendicular to σ_1 because [0 0 1] is the fastest growth direction for CAS.[28,29]

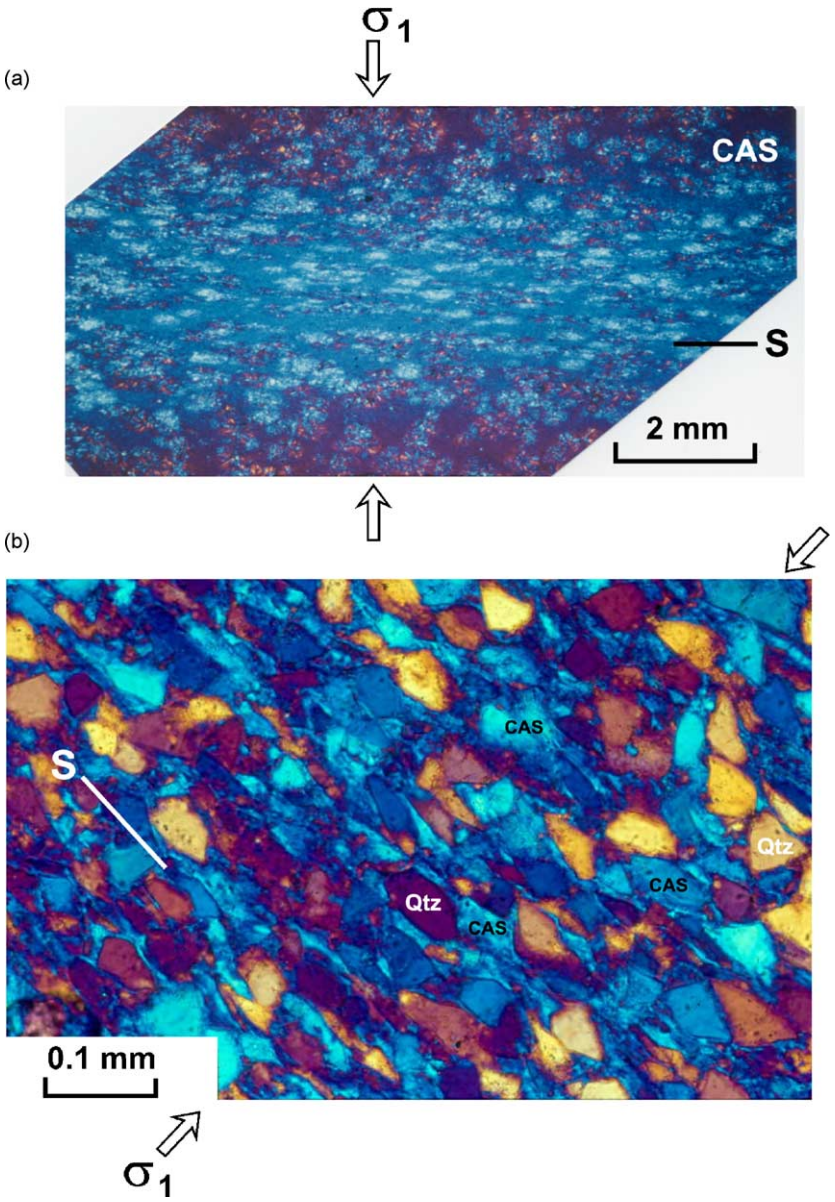

Fig. 10. Optical microstructures of deformed samples. Crossed polarizers with an auxiliary gypsum plate. The different colors reflect different crystallographic orientations. (a) A CAS layer from a layered composite (sample J22) shortened axially at 300 MPa, 1373 K, $10^{-5}\,s^{-1}$ and 32% strain. (b) A particulate composite (sample J14) containing 50 vol.% quartz (coarse clasts) and 50 vol.% CAS (fine grains), shortened axially at 300 MPa, 1273 K, $10^{-5}\,s^{-1}$ and 31% strain. The foliation (S) is perpendicular to the compression direction (σ_1). The blue CAS grains align their (0 1 0) and [1 0 0] nearly parallel to the foliation.

The PC samples are characterized by a plastically flowing CAS matrix containing almost rigid Qtz clasts (Fig. 10b). The CAS laths and polycrystalline fibers developed a marked foliation that is deflected around large Qtz clasts in which undulatory extinction is the sole feature of incipient plastic deformation. Measurements show that Qtz has almost same average grain size and aspect ratio in deformed (Fig. 12) and undeformed (Fig. 3) particulate composites, confirming that Qtz grains have not deformed plastically. EBSD measurements of Qtz grains from a PC aggregate (sample J14) shortened 31% at 1273 K and a constant strain rate of $10^{-5}\,s^{-1}$ show no preferred orientation of poles to $\{1\,0\,\bar{1}\,0\}$, $\{1\,1\,\bar{2}\,0\}$ and $\{1\,1\,\bar{2}\,1\}$. Hence the observed shape preferred orientation of Qtz (Fig. 10b) is most likely due to rigid rotations of elongate grains in the axially compressive strain field. In contrast, the CAS matrix developed a strong CPO as indicated by the optically parallel extinction or uniform color in cross polarized light with an auxiliary gypsum plate (Fig. 10b), which can be also interpreted as the result of dislocation slip on the (0 1 0)[1 0 0] system. Our optical observations qualitatively suggest that CAS in the particulate composites containing 50 vol.% Qtz develops the same pattern and strength of CPO as that in pure CAS aggregates, if we compare samples which deformed at the same conditions

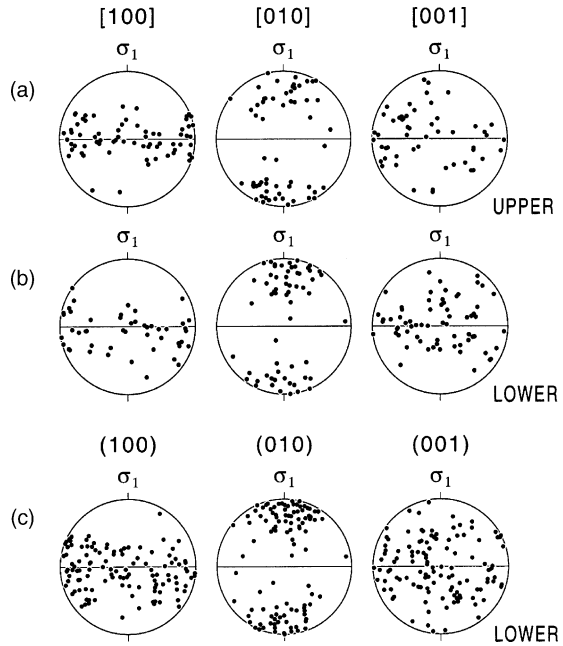

Fig. 11. Crystallographic preferred orientation (CPO) of CAS from a CAS layer shortened to 52%. Foliation (horizontal line) is perpendicular to the compression direction (σ_1). Notice that the whole sphere, rather than a hemisphere, is necessary to represent the distribution of the positive directions. Projections of [0 0 1], [0 1 0] and [1 0 0] on the upper (a) and lower (b) hemispheres. (c) Lower hemisphere projections of poles to (0 0 1), (0 1 0) and (1 0 0). Stereonets are equal-area plots. One hundred and thirty measurements are used.

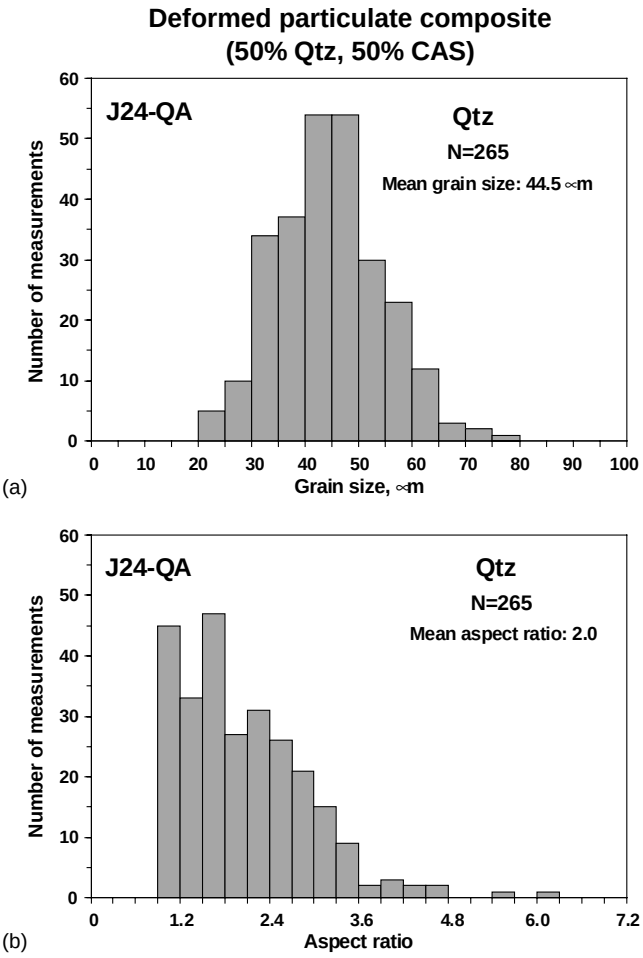

Fig. 12. Grain size distribution of quartz in a particulate composite (J24-QA) containing equal volume fractions of quartz and CAS, shortened axially at 300 MPa, 1373 K, $10^{-5}\,s^{-1}$ and 23% strain. Measurements were made from optical photomicrographs.

and have undergone the same type and magnitude of strain. The addition of Qtz into the CAS matrix appears to have two separate but antagonist effects on CAS texture. On the one hand, rigid Qtz clasts cause complex flow in adjacent CAS matrix, producing deflected foliation and local variations in the texture around the Qtz clasts and accordingly diffusing the overall pattern of the texture and attenuating the texture intensity of CAS. On the other hand, the CAS has to undergo nearly twice as much strain to accomplish the same total strain of sample because Qtz is almost undeformed in the particulate composites; such a strong strain partitioning tends to increase the texture intensity of CAS. A combination of the above effects results that the addition of rigid Qtz grains does not cause a discernible change in either the CPO pattern or the CPO intensity of CAS.

TEM observations show that CAS grains from the pure CAS aggregates, particulate composites or the CAS layers of Qtz–CAS layered composites have very similar microstructural characteristics. The CAS grains display variable dislocation densities with very high densities ($>5 \times 10^{14}\,m^{-2}$) in relict grains and very low densities ($5 - 8 \times 10^{11}\,m^{-2}$) in recrystallized neograins (Fig. 13). Even within the grains with very high dislocation densities, the distribution of dislocations is heterogeneous, with dislocations clustered along narrow planar zones that are generally parallel to (0 1 0) planes, forming so-called cells.[13,14] The cells could be formed by the interaction of more active glide dislocations (i.e., (0 1 0)[1 0 0]) with less mobile forest dislocations (e.g., (0 1 0)[0 0 1], (0 0 1)[1 0 0] and (1 1 0)[0 0 1]) and by the interaction between gliding dislocations and mechanical twins. The planar zones of high dislocation densities indicate that the (0 1 0) plane is a main slip plane under the conditions of investigation. Furthermore, the deformed CAS developed strongly sutured grain boundaries with neograins bulging from regions with very high dislocation densities to areas with low dislocation densities.[30] No well-developed subgrain boundaries or dislocation walls have been observed.

5. Discussion

5.1. Flow strength

One of the major problems with the high temperature structural applications of pure CAS aggregates is their relatively low flow strength at high temperatures. The present study provides one way of overcoming this problem by

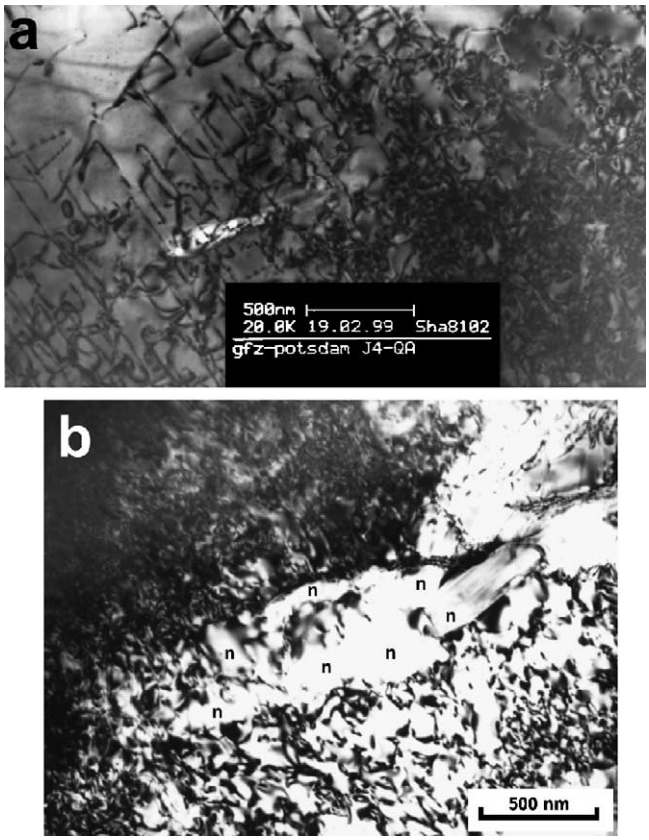

Fig. 13. TEM (bright field) micrographs showing typical substructures of dislocations in deformed CAS grains from sample J4-QA (particulate composite deformed by axial compression at 300 MPa, 1373 K, $10^{-5}\,s^{-1}$ and 29% strain). The distribution of dislocations is heterogeneous. (a) Two sets of dislocations that are tangled are observed in a plane nearly parallel to (0 1 0). (b) Grain boundary migration toward highly strained grains with very high (tangled) dislocation density, forming recrystallized neograins (n).

introducing quartz grains in the CAS matrix as either particulate or layered reinforcements. Ceramic composites of these sorts can be easily prepared by hot-pressing or sintering. Quartz is inexpensive and also has the advantage that it is chemically stable and does not react with CAS up to the eutectic melting point. Relative to the monolithic CAS aggregates, the overall compressive flow strength for the particulate composites with equal volume fractions of quartz and CAS increases more than fourfold, and that for the layered composites of the same composition increases substantially with decreasing the thickness of the layers. For instance, the layered composites with $d/h = 9$ have an overall flow strength 10 times higher than that of the monolithic CAS aggregates. In both particulate and layered composites, quartz is essentially rigid in the plastic CAS matrix. The above results are the principal mechanical findings of this study.

The layering-induced hardening of Qtz–CAS multilayers can be interpreted by taking into account the following mechanical processes:

(i) In a composite, the softer phase deforms at a greater strain rate ($\dot{\varepsilon}_{is}$) than the bulk strain rate of the composite, $\dot{\varepsilon}_c$. Then the in situ softer phase in the composite has a higher resistance to plastic flow (σ_{is}) than the same material in bulk form (σ_0). This effect can be evaluated by taking account of relative strain amounts partitioned between the Qtz and CAS layers using

$$\sigma_{is} = \sigma_0 \left(\frac{\dot{\varepsilon}_{is}}{\dot{\varepsilon}_c}\right)^{1/n} \quad (1)$$

where n is the stress exponent. The hardening effect is more pronounced when n has a smaller value than a larger value.

(ii) Flow of the soft phase in a composite is constrained by the hard phase. As a result, the in situ response of the soft phase is hardened relative to its single phase aggregate.[31] The compressive flow strength of the constrained weak layer (σ_w) is higher than the compressive flow strength without constraint or in the monolithic aggregate (σ_0) at a given plastic strain,[32]

$$\sigma_w = 2\sigma_0 \left(\mu\frac{d}{h}\right)^{-2}\left[\exp\left(\mu\frac{d}{h}\right) - \mu\frac{d}{h} - 1\right] \quad (2)$$

where μ is the friction coefficient of the interface between the strong and weak layers, d and h are the diameter and thickness of the weak layer. For a given μ, even though it is as small as 0.25, increasing the diameter-to-thickness ratio (d/h) of the layer easily leads to a significant increase in its resistance to compressive plastic deformation. Taking into account the above two effects described by Eqs. (1)–(2), we can readily explain the hardening of the Qtz–CAS layered composites with respect to the bulk strength of monolithic CAS.

5.2. Constant load creep tests under uniaxial compression versus constant strain-rate deformation tests under axial compression

Most of the previous uniaxial creep tests[5,8–11] were performed under constant load and at ambient pressure, where the CAS samples have a significant increase in porosity because there is no sufficient confining pressure to hinder the creep-induced cavitation. For example, Nair et al.[11] showed 8% axial strain resulted in an increase in porosity to 24% in their CAS-II specimens. Furthermore, their microstructural analysis suggested no significant difference in grain morphology between deformed and undeformed samples. The cavitation at the grain boundaries could be the dominant deformation mechanism for the previous creep tests conducted at ambient pressure. However, our experiments on the deformation of the CAS aggregates and CAS–Qtz composites were carried out at a confining pressure of 300 MPa, where cavitation could not occur. TEM observations and textural analysis strongly suggest that the plastic deformation of CAS under the experimental conditions is dominated by dis-

location creep accommodated by grain boundary migration recrystallization.

There is also doubt that steady-state creep has truly achieved at each step of stress change after a strain as small as only 1–3% during the previous uniaxial creep tests. Our constant strain-rate tests under axial compression at a confining pressure of 300 MPa (e.g., samples J4, J13, J14 and J25) show a continuous variation of flow stress with increasing strain up to 65%, indicating that no steady-state creep has reached because the microstructure of the material evolves continuously toward large strain. Torsion experiments[12,22] also display that the sample strength varies continuously with the microstructural evolution toward large strains. It is possible that during a traditional load-constant creep test the strain rate, when the time–strain curve first flattens out, is inappropriately taken as the steady-state strain rate. Thus, there could be substantial discrepancies between experimental results from load-constant creep and constant strain-rate deformation tests. We believe that a better understanding of the discrepancies and their cause(s) is an important prerequisite to the correct interpretation of the mechanical data of material deformation tests. Thus this should be motivation of our further study.

5.3. Dominant slip system of CAS

CAS grains show a random CPO in undeformed, HIPed aggregates. In both monolithic and composite aggregates deformed by axial compression, however, CAS grains develop strong CPO with the poles to (0 1 0) at the maximum compression axis (σ_1) and a girdle of [1 0 0] normal to σ_1. The numerical models of axial compression,[33,34] in which only one slip system is available to each grain, predicts that the slip plane tends to align parallel to the flattened foliation plane that is perpendicular to the maximum compression direction while the slip direction tends to align in the foliation plane with increasing compressive strain. Thus, (0 1 0)[1 0 0] provides an "easy slip" system for CAS under our experimental conditions.

In CAS, the strongest bonds are the Al–O and Si–O tetrahedral or T–O bonds. To a first approximation, the easiest glide planes will be those intersecting the smallest number of T–O bonds per unit area. Using this criterion, the easiest glide planes in CAS should be (0 1 0) with two T–O bonds per unit cell, followed by (0 0 1), (1 1 0), ($\bar{1}\,\bar{1}$ 0) and (1 0 $\bar{1}$) with four each, and then (1 0 0) and (1 1 1) with six. The easiest slip direction will be the shortest Burgers vector because dislocations with the shortest Burgers vector have the lowest energy and in turn the most stable. If we restrict ourselves to possible Burgers vectors in the easiest glide plane (0 1 0), then we would expect 1/2[0 0 1] with $\vec{b} = 0.7$ nm which is dissociated and [1 0 0] with $\vec{b} = 0.8$ nm. Thus it is likely that a transition from dominant c-slip to a-slip on (0 1 0) planes occurs as a function of deformation conditions. It is expected that c-slip prevails at moderate temperature (550–900 °C), high pressure (>800 MPa), low strain-rate ($<10^{-12}$ s^{-1}) and relatively low H_2O content[20,30,35–37] while a-slip is dominant at high temperature (>1000 °C), low–moderate pressure (<600 MPa), high strain-rate ($>10^{-9}$ s^{-1}) and relatively high H_2O content.[22]

In triclinic CAS, there are certainly no enough independent slip systems to produce either homogeneous or arbitrary deformation in its polycrystal. Many features in our deformed samples such as inhomogeneous dislocation density and grain boundary migration recrystallization all indicate heterogeneous strain. High densities of dislocations result from interaction between dominant (0 1 0)[1 0 0] system and other secondary slip systems such as (0 1 0)[0 0 1], (0 1 0)[1 0 1] and (0 0 1)[1 0 0]. As just one dominant slip system and a few secondary slip systems can be activated, strain will lead to lattice rotation and rapid formation of strong CPO. The texture analysis suggests that CAS deform largely by slip on just one dominant system, (0 1 0)[1 0 0], while mechanical twinning, anisotropic growth and particularly grain boundary migration recrystallization play an role to relieve the incompatibilities which would otherwise result from such limited slip systems.

6. Conclusions

The mechanical behavior of layered and particulate composites of calcium aluminosilicate and SiO_2 (quartz) with equal volume fractions and that of the end-member materials have been investigated by axial compression ($\sigma_1 > \sigma_2 = \sigma_3 > 0$) at a confining pressure ($\sigma_2 = \sigma_3$) of 300 MPa, strain rates of 10^{-5} to 10^{-4} s^{-1} and temperatures from 1173 to 1473 K. All the samples were made by hot isostatical pressing of quartz crystalline and CAS glass powders into dense crystalline aggregates. Under the experimental conditions, the CAS, whenever occurs in the monolithic aggregates or in the composites, exhibit consistently TEM microstructures indicative of dislocation creep accommodated by dynamic recrystallization. The latter occurs by bulging and migration of grain boundaries through the highly strained mantle, giving rise to a mosaic of strain-free new grains. The HIPed samples exhibit no discernible CPO for CAS whereas the axially shortened CAS aggregates or layers develop a strong CPO with the normal to (0 1 0) parallel or subparallel to the maximum compression axis (σ_1) while the [1 0 0] direction aligned in the σ_1-normal flattening foliation. Clearly, the texture formed during the experimental deformation rather inherited from the HIP. Since there is no reason for diffusion creep to induce any CPO,[38] the texture should be formed by dislocation glide. The CPO pattern indicates that in CAS, [1 0 0] slip is significantly easier than [0 0 1] slip on the easiest slip plane (0 1 0) under the experimental conditions. Quartz is almost rigid under the experimental conditions.

The flow strengths of both monolithic CAS and SiO_2/CAS composites are strongly influenced by strain rate and temperature, increasing with an increase in strain rate and a decrease in temperature. Particulate and particularly layered

composites are significantly stronger than monolithic CAS aggregates, indicating that quartz is an effective reinforcement to the CAS matrix even when the material is used at high temperatures. Under layer-normal compression, the flow strength of layered composites increases remarkably with decreasing the thickness of the compositional layers. Under the same conditions, the thin-layered composites are significantly stronger than particulate counterparts with the same composition. The observed layering-induced hardening of two-phase composites is due to constraint effects of rigid quartz on plastic flow of CAS.

Acknowledgements

The NSERC of Canada, the Alexander von Humboldt Foundation of Germany, and Chinese Academy of Sciences (KZCX2-SW-117) supported this research. We thank G. Dresen, M.S. Paterson, D. Prior for helpful discussion, Michael Naumann for technical assistance with high *T* and high *P* experiments, Stefan Gehrmann for preparation of thin sections, and A. Lacombe for drawing figures.

References

1. Wendt, A. S., Olgaard, D. L. and Mainprice, D., A technique for the fabrication of fully dense Ca-rich plagioclase (An_{70}–An_{100}) samples suitable for studying the plastic rheology of bytownite (An_{80}). *J. Mater. Sci.* 1999, **34**, 5733–5742.
2. Brennen, J. J. and Prewo, K. M., Silicon carbide-fiber-reinforced glass-ceramic-matrix composites exhibiting high strength and toughness. *J. Mater. Sci.* 1982, **17**, 371–383.
3. Sung, Y. M. and Hwang, S. J., Microstructural analysis of the calcium aluminosilicate (CAS) glass-ceramic matrix in SiC_f/CAS composites deformed at a high temperature. *J. Mater. Sci.* 1998, **33**, 5255–5258.
4. Lo, C. L., Duh, J. G. and Chiou, B. S., Low temperature sintering and crystallization behavior of low loss anorthite-based glass-ceramics. *J. Mater. Sci.* 2003, **38**, 693–698.
5. Ji, S. C., *Déformation Plastique Naturelle et Expérimentale des Plagioclases.* Ph.D. thesis, Université de Montpellier II, France, 1987.
6. Mercier, R. F. and Chokshi, A. H., The elevated temperature compression creep behaviour of a calcium aluminosilicate (anorthite) glass-ceramic. *Scr. Metall. Mater.* 1993, **28**, 1177–1182.
7. Meyer, D. M., Cooper, R. F. and Plesha, M. E., High-temperature creep and the interfacial mechanical response of a ceramic matrix composite. *Acta Metall. Mater.* 1993, **41**, 3157–3170.
8. Wang, Z., Dresen, G. and Wirth, R., Diffusion creep of fine-grained polycrystalline anorthite at high temperature. *Geophys. Res. Lett.* 1996, **23**, 3111–3114.
9. Dimanov, A., Dresen, G. and Wirth, R., High-temperature creep of partially molten plagioclase aggregates. *J. Geophys. Res.* 1998, **103**, 9651–9664.
10. Dimanov, A., Dresen, G., Xia, X. and Wirth, R., Grain-boundary diffusion creep of synthetic anorthite aggregates: the effect of water. *J. Geophys. Res.* 1999, **104**, 10483–10497.
11. Nair, B. G., Cooper, R. F., Bruhn, D. B. and Kohlstedt, D. L., High-temperature rheology of calcium aluminosilicate (anorthite) glass-ceramics under uniaxial and triaxial loading. *J. Am. Ceram. Soc.* 2001, **84**, 2617–2624.
12. Bystricky, M., Kunze, K., Burlini, L. and Burg, J. P., High shear strain of olivine aggregates: rheological and seismic consequences. *Science* 2000, **290**, 1564–1567.
13. Ji, S. C. and Mainprice, D., Experimental deformation of sintered plagioclase above and below the order-disorder transition. *Géodinam. Acta* 1987, **1**, 113–124.
14. Tullis, J. and Yund, R., Dynamic recrystallization of feldspar: a mechanism for ductile shear zone deformation. *Geology* 1985, **13**, 238–241.
15. Tullis, J. and Yund, R. A., Diffusion creep in feldspar aggregates: experimental evidence. *J. Struct. Geol.* 1991, **13**, 987–1000.
16. Rybacki, E. and Dresen, G., Dislocation and diffusion creep of synthetic anorthite aggregates. *J. Geophys. Res.* 2000, **105**, 26017–26036.
17. Heidelbach, F., Post, A. and Tullis, J., Crystallographic preferred orientation in albite samples deformed experimentally by dislocation and solution precipitation creep. *J. Struct. Geol.* 2000, **22**, 1649–1661.
18. Wenk, H. R., Bunge, H. J., Jansen, E. and Pannetier, J., Preferred orientation of plagioclase: neutron diffraction and U-stage data. *Tectonophysics* 1986, **126**, 271–284.
19. Xie, Y. X., Wenk, H. R. and Matthies, S., Plagioclase preferred orientation by TOF neutron diffraction and SEM-EBSD. *Tectonophysics* 2003, **370**, 269–286.
20. Ji, S. and Mainprice, M., Natural deformation fabrics of plagioclase: implications for slip systems and seismic anisotropy. *Tectonophysics* 1988, **147**, 145–163.
21. Prior, D. and Wheeler, J., Feldspar fabrics in a greenschist facies albite-rich mylonite from electron backscatter diffraction. *Tectonophysics* 1999, **303**, 29–49.
22. Ji, S., Jiang, Z. and Wirth, R., Crystallographic preferred orientation (CPO) of experimentally sheared plagioclase aggregates: implications for crustal heterogeneity (abstract). *Eos Trans. AGU* 1999, **80**, 916.
23. Jiang, Z. T., Prior, D. J. and Wheeler, J., Albite crystallographic preferred orientation and grain misorientation distribution in a low-grade mylonite: implications for granular flow. *J. Struct. Geol.* 2000, **22**, 1663–1674.
24. Underwood, E. E., *Quantitative Stereology*. Addison-Wesley, Reading, MA, USA, 1970.
25. Abe, T., Tsukamoto, K. and Sunagawa, I., Nucleation, growth and stability of $CaAl_2Si_2O_8$ polymorphs. *Phys. Chem. Miner.* 1991, **17**, 473–484.
26. Lofgren, G., An experimental study of plagioclase crystal morphology: isothermal crystallization. *Am. J. Sci.* 1974, **274**, 243–273.
27. Franke, W. and Ghobarkar, H., The morphology of hydrothermally grown plagioclase. *Crystal Res. Technol.* 1982, **17**, 459–464.
28. Klein, L. and Uhlmann, D. R., Crystallization behaviour of anorthite. *J. Geophys. Res.* 1974, **79**, 4869–4874.
29. Shelley, D., *Igneous and Metamorphic Rocks Under the Microscope*. Chapman & Hall, New York, USA, 1993.
30. Ji, S. C. and Mainprice, D., Recrystallization and fabric development in plagioclase. *J. Geol.* 1990, **98**, 65–79.
31. Poech, M. H. and Fischmeister, H. F., Deformation of two-phase materials: a model based on strain compatibility. *Acta Metall. Mater.* 1992, **40**, 487–494.
32. Unksov, E. P., *An Engineering Theory of Plasticity*. Butterworths, London, 1961.
33. Etchecopar, A., A plane kinematic model of previous deformation in a polycrystalline aggregate. *Tectonophysics* 1977, **39**, 121–139.
34. Etchecopar, A. and Vasseur, G., A 3-D kinematic model of fabric development in polycrystalline aggregates: a comparison with experimental and natural examples. *J. Struct. Geol.* 1987, **9**, 705–717.
35. Olsen, T. S. and Kohlstedt, D. L., Analysis of dislocations in some naturally deformed plagioclase feldspar. *Phys. Chem. Mineral.* 1984, **11**, 153–160.
36. Ji, S. C., Mainprice, D. and Boudier, F., Sense of shear in high-temperature movement zones from the fabric asymmetry of plagioclase feldspars. *J. Struct. Geol.* 1988, **10**, 73–81.
37. Stünitz, H., Fitz Gerald, J. D. and Tullis, J., Dislocation generation, slip systems and dynamic recrystallization in experimentally deformed plagioclase single crystals. *Tectonophysics* 2003, **372**, 215–233.
38. Karako, S. I. and Wu, P., Rheology of upper mantle: a synthesis. *Science* 1993, **260**, 771–778.